ENSO and the Spatial Extent of Interannual Precipitation Extremes in Tropical Land Areas

BRADFIELD LYON AND ANTHONY G. BARNSTON

International Research Institute for Climate Prediction, Lamont-Doherty Earth Observatory, Columbia University, Palisades, New York

(Manuscript received 6 July 2004, in final form 13 June 2005)

ABSTRACT

The extreme phases of El Niño–Southern Oscillation (ENSO) are known to dominate the interannual variability of tropical rainfall. However, the relationship between ENSO and the *spatial extent* of drought and excessively wet conditions is an important characteristic of the tropical climate that has received relatively less attention from researchers. Here, a standardized precipitation index is computed from monthly rainfall analyses and the temporal variability of the spatial extent of such extremes, for various levels of severity, is examined from a Tropics-wide perspective (land areas only, 30°S–30°N). Maxima in the spatial extent of both precipitation extremes are compared across multiple ENSO events that occurred during the period 1950–2003. The focus on tropical land areas is motivated by the numerous, often negative, impacts of ENSO-related precipitation variability on human populations.

Results show that major peaks in the spatial extent of drought and excessively wet conditions are generally associated with extreme phases of ENSO. A remarkably robust linear relationship is documented between the spatial extent of drought in the Tropics and El Niño strength (based on Niño-3.4 sea surface temperature anomalies), with a comparatively weaker relationship for La Niña and excessive wetness. Both conditions are found to increase by about a factor of 2 between strong and weak ENSO events, and in several locations they are shown to be more likely during ENSO events than at all other times, especially for severe categories. Relatively stronger El Niño events during recent decades are associated with increased drought extent in tropical land areas with increasing surface temperatures likely acting to exacerbate these dry conditions.

1. Introduction

The association between El Niño–Southern Oscillation (ENSO) warm and cold events and interannual precipitation extremes in various teleconnected regions of the globe is well established (Ropelewski and Halpert 1987; Kiladis and Diaz 1989). However, the spatial extent of ENSO-related precipitation anomalies and its variability among different events are important characteristics of the phenomena that have not been examined in detail, particularly in the Tropics where the ENSO signal is largest. Of particular interest are interannual precipitation variations over land areas since they are frequently associated with multiple and often deleterious consequences for both human populations and the environment. For example, Dilley and Heyman (1995) have shown that for several tropical countries drought disasters are twice as likely to be declared in the year following an El Niño event. Of course in some locations excessively wet (dry) conditions are also associated with El Niño (La Niña) but, on average, drought is more common during El Niño with excessively wet conditions generally more widespread during La Niña when all tropical land areas are considered (e.g., Mason and Goddard 2001). Documenting the large-scale, spatially integrated precipitation response to the extreme phases of ENSO in tropical land areas is the main focus of the current study, with the consistency of that response examined across multiple ENSO events.

Previous studies that have considered the spatial extent of ENSO-related precipitation anomalies have tended to be either globally or regionally focused, and have not explicitly looked at its variability with specific ENSO events. Dai et al. (1998) examined the temporal variability in the spatial coverage of severe aridity and

Corresponding author address: Dr. Bradfield Lyon, International Research Institute for Climate Prediction, Lamont-Doherty Earth Observatory, Columbia University, Monell Bldg., Palisades, NY 10964.
E-mail: blyon@iri.columbia.edu

wetness conditions for various regions of the globe based on a gridded analysis of the Palmer Drought Severity Index (PDSI). Their analysis did not examine the Tropics as a distinct region but their EOF analysis of global PDSI did indicate a statistically significant ENSO signal. In addition, they noted that since roughly 1980 there has been an increase in the areal extent of wet and dry extremes in several ENSO-affected regions. Analyzing observed, standardized annual precipitation anomalies for the globe, Dai et al. (1997) found, among other results, a positive correlation between time series of the areal extent of precipitation extremes (more than one standard deviation from the mean) and their relative severity for various regions, including the Tropics. Recently, Dai et al. (2004) presented an updated version of the PDSI dataset with time series of the spatial extent of very dry or wet conditions across several tropical regions affected by ENSO. In addition to indicating an upward trend in the spatial coverage of drought in global land areas (60°S–60°N), they provided maps of the geographical distribution of the trends for the globe. And Mason and Goddard (2001) estimated the average spatial extent of the globe with ENSO-related seasonal precipitation extremes (defined as the two outer tercile classes) but they did not examine its variability between ENSO events nor did they consider the Tropics separately.

Recently Lyon (2004) reported that the spatial extent of drought (identified by 12-month accumulated precipitation anomalies), when measured across all tropical land areas, was closely related to the strength of El Niño events (determined by associated maxima in Niño-3.4 SST anomalies[1]). The study showed that drought extent increased by roughly a factor of 2 between weak and strong El Niño events in a near-linear fashion, a relationship that did not change significantly with drought severity.

This study extends the work of Lyon (2004) to consider the spatial extent of excessively wet and dry conditions throughout all tropical land areas during both extreme phases of ENSO (i.e., warm and cold ENSO events). The association with the relative strength of individual ENSO events will also be evaluated. Is there a robust relationship between ENSO cold events and the spatial extent of excessively wet conditions in the Tropics? How does this relationship compare to that for El Niño and drought? To what extent do ENSO extremes influence the likelihood of drought or excessive rainfall at a given location? These are some of the motivating questions behind the study.

[1] SST anomalies were averaged across the Niño-3.4 region (5°S–5°N, 120°–170°W).

Section 2 describes the rainfall analyses used in the study, the standardized precipitation index used to identify interannual extremes in precipitation, and the overall methodology. Results of the analysis for the spatial extent of both wet and dry extremes are presented in section 3, with a summary and discussion of overall findings given in section 4.

2. Data and methodology

a. Data

The primary dataset used in the study is the gridded, monthly precipitation analysis for the globe (land regions only) provided by the University of East Anglia (UEA) (New et al. 1999, 2000). This analysis is based on precipitation measured at land-based observing stations around the globe that is quality controlled before being interpolated onto a 0.5° × 0.5° resolution latitude–longitude grid. These data have been used extensively in climate studies and formed the basis of the recent probabilistic assessment of ENSO-related precipitation anomalies by Mason and Goddard (2001). UEA data for the period January 1950–December 1998 were utilized here. To extend the analysis through 2003, monthly gridded precipitation analyses for the globe were obtained from the Climate Prediction Center's Merged Analysis of Precipitation (CMAP) (Xie and Arkin 1996) covering the period January 1979–December 2003. To test the robustness of the main findings presented, results obtained from supplemental datasets were compared with those obtained from the UEA data. Of course, since many of the same observing stations are used in the construction of various rainfall analyses, different analyses do not truly represent independent estimates of observed precipitation. However, different data inputs, gridding, or merging techniques are employed across various precipitation analyses, allowing for some measure of variation. With this in mind, the CMAP results were compared with those obtained using the Global Precipitation Climatology Project (GPCP) precipitation analysis (Huffman et al. 1997), which covers the same period and spatial domain. The CMAP and GPCP precipitation analyses are both constructed by merging observed rainfall (i.e., gauge data) measurements with satellite estimates through related, though differing, methodologies (Yin et al. 2004). Naturally, over the ocean these analyses depend on estimates from satellite given the very small number of observing stations on atolls and small islands. Twenty-five-year linear trends were removed from the GPCP and CMAP rainfall estimates over ocean areas prior to being analyzed. A final comparison with the UEA results was made by utilizing the Pre-

cipitation Reconstruction over Land (PRECL) dataset, which consists of monthly precipitation analyses for global land areas based solely on gauge data (Chen et al. 2002). The CMAP, GPCP, and PRECL analyses are all at a 2.5° × 2.5° spatial resolution. Finally, the Dai et al. (1998) global dataset of PDSI for the period 1950–98 was used as a reference for the drought/extreme wetness conditions identified by the standardized precipitation index used here. The available version of the PDSI dataset (2.5° × 2.5° resolution) lacked complete spatial coverage in the Tropics and therefore could not be used as a primary data source for the type of analysis considered in this study.

Monthly sea surface temperature (SST) data were obtained from the extended reconstruction of global SST developed by Smith and Reynolds (2003) and are on a 2.0° × 2.0° resolution grid, with a 1961–90 climatological base period used to compute monthly anomalies. Data for January 1950–December 2003 were used in the analysis. Atmospheric data used in the study are from the National Centers for Environmental Prediction–National Center for Atmospheric Research (NCEP–NCAR) reanalysis (Kistler et al. 2001), and all data were accessed via the International Research Institute (IRI) Data Library (available online at http://iridl.ldeo.columbia.edu/).

b. Computing a standardized precipitation index

To measure interannual precipitation extremes, a standardized precipitation index was computed at all grid points in tropical land areas from 30°S to 30°N. The index, referred to as the weighted anomaly of standardized precipitation (WASP), is based on overlapping N-month sums of weighted, standardized monthly precipitation anomalies, S_N, where

$$S_N = \sum_{i=1}^{N} \left(\frac{P_i - \overline{P_i}}{\sigma_i} \right) \frac{\overline{P_i}}{\overline{P_A}}. \quad (1)$$

In (1) P_i and $\overline{P_i}$ are the observed and climatological values of precipitation, respectively, for the ith month relative to the month/year when an index value is being computed (where $i = 1$ is the current month, $i = 2$ is the previous month, etc.). A time series of this sum has overlapping monthly inputs since the ending month progresses forward in 1-month increments. The standard deviation of monthly precipitation is given by σ_i. The base period used for computing climatological values was 1961–90 (1979–2003 for CMAP and GPCP data). The mean annual precipitation for a given grid point is indicated by $\overline{P_A}$ and the weighting factor, $\overline{P_i}$ / $\overline{P_A}$, is used to dampen large standardized anomalies that result from small precipitation amounts occurring near the start or end of dry seasons and to emphasize anomalies during the heart of rainy seasons. In this study the focus is on interannual precipitation variability, so $N = 12$. The sum S_{12} has itself been standardized to obtain a dimensionless measure of the relative severity of precipitation surplus or deficit, given symbolically as WASP_{12}:

$$\mathrm{WASP}_{12} = \frac{S_{12}}{\sigma_{S_{12}}}. \quad (2)$$

Time series of the WASP_{12} index, at 1-month increments, were computed from December 1950 to December 1998 and from December 1979 to December 2003, for the East Anglia and CMAP data, respectively. The index is highly correlated with, though not numerically equal to, a 12-month standardized precipitation anomaly. Since temporal variations in the WASP_{12} index at a given grid point reasonably fit a normal distribution,[2] index values typically range from −2.0 (severe drought) to +2.0 (severe wetness) and the qualifiers *moderate*, *intermediate*, and *severe* are used here to describe WASP_{12} magnitudes exceeding ±1.0, ±1.5, and ±2.0, respectively. Desert regions, defined as having climatological precipitation of less than 96 mm yr^{-1}, are masked from the analysis. This threshold was chosen in order to approximately match, visually, the "dry" mask with the driest desert regions of the world as shown in Hartman (1994). The results were not highly sensitive to the specific threshold chosen.

The WASP_{12} index is well correlated with the PDSI as shown in Fig. 1 where area averages of both indices have been computed to create corresponding time series for several randomly selected regions of the Tropics. For reference, the PDSI typically ranges between −6 (extreme drought) to +6 (extreme wetness). The tropical average pattern correlation was 0.6, although it is noted that in only 69% of the Tropics was PDSI data available for at least 75% of the time of the comparison period. The high temporal correlations between indices indicate the dominant role of precipitation anomalies in affecting variations in the PDSI despite the importance of other factors, such as surface air temperature (e.g., Hu and Wilson 2000), which can be significant when examining longer-term secular trends (e.g., Dai et al.

[2] The index does have a tendency to be somewhat positively skewed, particularly in semiarid regions. About 20% (13%) of grid points in tropical land areas displayed a skewness significantly different from zero at the 95% (99%) confidence level, with the largest spatially coherent region being in the Australian desert region.

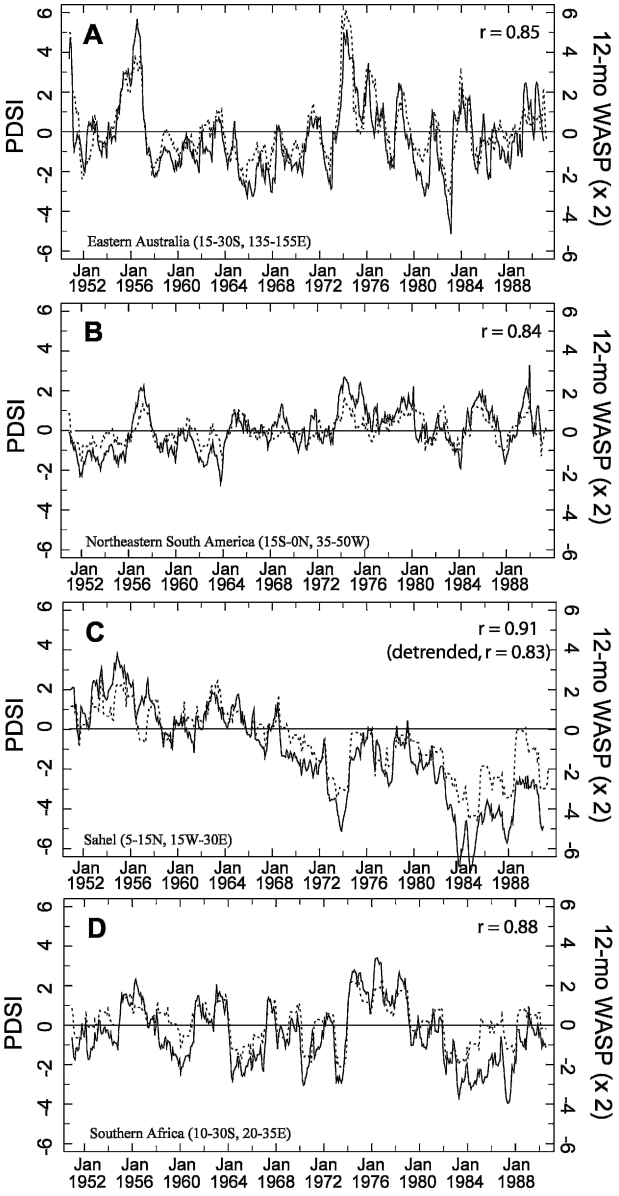

FIG. 1. Time series of monthly values of the PDSI (solid line) and $WASP_{12}$ index (dashed line, values multiplied by 2) averaged over randomly chosen tropical regions for the period 1950–90. Linear correlations are shown in the upper right of each plot; geographic regions on the bottom left.

2004). However, $WASP_{12}$ appears to be a good proxy for soil moisture variability on shorter time scales to the extent that this is realistically captured by the PDSI (Alley 1984) and has the advantage of being much more easily computed.

An important attribute of the $WASP_{12}$ index is the monthly weighting factor, which effectively eliminates dry seasons and allows for the spatially integrated effect of ENSO on interannual precipitation extremes across the Tropics to be evaluated. For example, the average correlation between the October and following February values of $WASP_{12}$, averaged across all land areas 0°–30°N, is 0.88. The reason for this high correlation can be seen in Fig. 2 where the annual cycle of the zonally averaged, climatological rainfall (land areas only) is plotted along with the corresponding zonal averages of the $WASP_{12}$ weighting factor (both based on the UEA data). The tendency in Fig. 2 for maxima in the average weighting factor to be located poleward of maximum rainfall during extreme seasons is attributed to the relatively short length of the rainy season in locations near the maximum poleward extent of the summer monsoon systems, such as occurs in the northern Sahel during July. With dry seasons damped, the $WASP_{12}$ index is able to capture the influence of ENSO on the annual cycle of precipitation across rainy seasons of varying duration. While using a 12-month precipitation index may be suboptimal in some specific locations where rainfall (or ENSO forcing) does not follow such a simple annual cycle, tropical rainfall is dominated by the meridional movement of large-scale monsoon systems where the index works quite well, and the global-scale influence of ENSO across all tropical land areas is the primary focus of the current study.

c. The spatial extent of interannual precipitation extremes and ENSO definitions

Time series of the spatial extent of precipitation extremes were computed for all tropical land areas based on the three thresholds of the $WASP_{12}$ index. Thus, grid points where values of the index exceeded ± 1.0, ± 1.5, and ± 2.0 were flagged, weighted by the cosine of their latitude, and the fraction of total land area that they covered computed for each month. The date of distinct maxima in spatial extent was noted in each of the resulting six time series. The maxima in spatial extent were related to ENSO extremes by comparing their magnitude and date of occurrence to corresponding features of a time series of SST anomalies averaged over the Niño-3.4 region. A 5-month running average was applied to the Niño-3.4 SST time series, which covers the period January 1950–December 2003. The Niño-3.4 region was chosen since it is known to be the best region for monitoring changes in convection in the tropical Pacific associated with ENSO (Barnston et al. 1997). An El Niño (La Niña) event was identified when values of the Niño-3.4 SST time series were $>+0.4°C$ ($<-0.4°C$) for at least six consecutive months, a standard methodology for identifying ENSO events (e.g., Trenberth 1997). Using these criteria, El Niño (La Niña) conditions were observed 31% (24%)

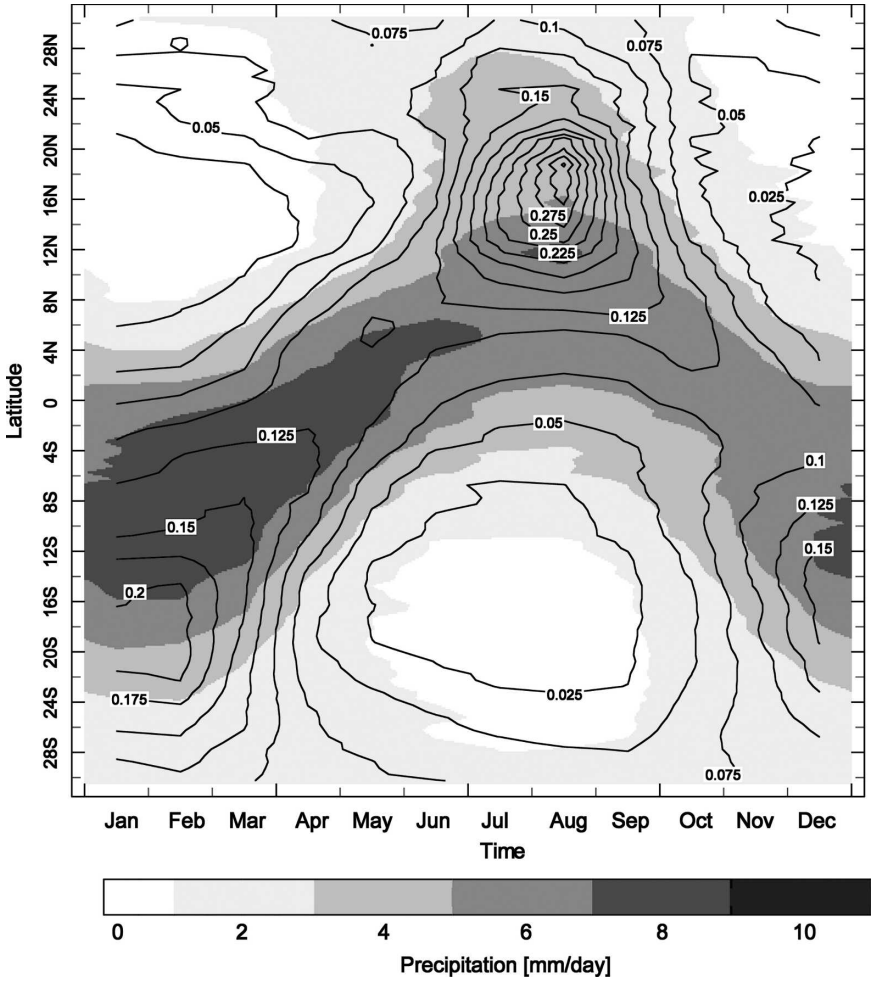

FIG. 2. Time–latitude section of the zonally averaged climatological precipitation (mm day^{-1}, shaded) for tropical land areas, and the average monthly values of the WASP weighting factor, $\overline{P_i}/\overline{P_A}$ (contours) based on the UEA data.

of the time between January 1950 and December 2003. Some general characteristics of the individual ENSO episodes identified in the study are listed in the appendix.

d. Data reliability

Since varying data inputs and methodologies are used in the construction of different gridded precipitation analyses, it was desirable to compare results derived from the UEA data with those obtained from other sources. A number of comparisons were made. For example, Fig. 3a indicates the percent of tropical land area where the $WASP_{12}$ index was less than -1.5 (i.e., "intermediate" drought) based on the UEA and PRECL data. The time series only extends to 1990 since the number of rainfall observations in the PRECL drops off dramatically after that time. Both time series in Fig. 3a capture similar peaks in the spatial extent of drought, and the rms difference in areal coverage between the two datasets was only 1.5%. Since the number of rainfall observations vary in time for the UEA data as well, a comparison with results after 1990 was based on similar time series computed from the CMAP and GPCP analyses (covering the period 1979–98), where satellite estimates of rainfall are blended with station data to obtain complete spatial coverage. These results are shown in Fig. 3b where all three of the time series are seen to be in good agreement, with generally similar magnitude of the peaks in drought extent across datasets. Similar results (not shown) were found when examining different levels of drought severity, and for the spatial extent of excessively wet conditions. Removing all grid points in coastal areas from the rainfall analyses prior to the spatial extent analysis had virtually no effect on the overall results.

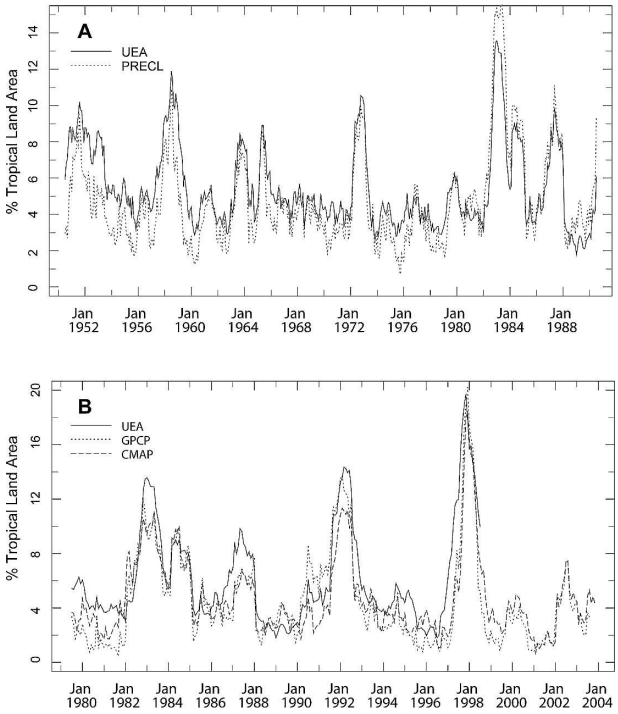

FIG. 3. (a) Time series (1950–90) of the percent of tropical land area where the $WASP_{12}$ index was ≤ -1.5 based on the UEA and PRECL precipitation analyses. (b) As in (a) but for the UEA, GPCP, and CMAP data for the period 1979–2003.

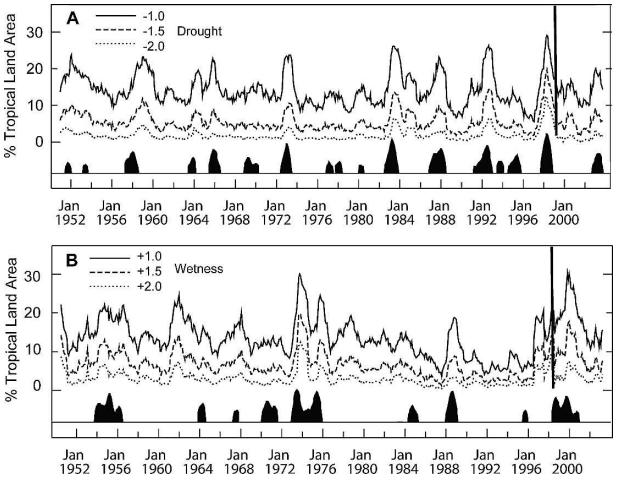

FIG. 4. Time series of the percentage of tropical land area experiencing (a) drought and (b) excessively wet conditions (1950–2003). Three categories of severity are plotted for each extreme: moderate ($WASP_{12} = \pm 1.0$; solid lines), intermediate ($WASP_{12} = \pm 1.5$, dashed lines), and severe ($WASP_{12} = \pm 2.0$, dotted lines). Shaded profiles at the bottom of each plot indicate the relative, absolute magnitude of monthly Niño-3.4 SST anomalies associated with individual (a) El Niño and (b) La Niña events. Time series values to the left (right) of the thick, vertical lines on the right side of the plots are based on UEA (CMAP) data.

3. Results

a. ENSO's connection to the spatial extent of interannual rainfall extremes

Time series of the spatial extent of moderate, intermediate, and severe drought and wetness conditions are plotted in Fig. 4 along with profiles of the relative magnitude of Niño-3.4 SST anomalies for individual warm and cold ENSO events. Most of the major peaks in spatial extent of drought and wetness are seen to correspond to, and lag, the peak magnitude of Niño-3.4 SST anomalies associated with individual El Niño and La Niña events. However, it is noted that appreciable peaks in the spatial extent of excessively wet conditions during 1961–62 and 1978 were not associated with La Niña events by the definition used here.

Using similar methods, Lyon (2004) showed the association between the spatial extent of drought and El Niño. Here, evidence is provided for the same qualitative behavior for excessively wet conditions during La Niña, with the average maximum spatial coverage of both wet and dry extremes apparently comparable. For reference, correlations exceeding ~0.6 (0.85) are statistically significant at the 90% (99.9%) confidence level based on a Fisher-Z transformation with $n - 3$ degrees of freedom (the area-average 12-month lag correlation of $WASP_{12}$ is only 0.08). Caution is urged when interpreting the results for excessively wet conditions. Even if a grid point is in the severe wetness category of the $WASP_{12}$ index, this does not necessarily imply flooding occurred at that location. Floods develop on much shorter time scales (often less than a month) than the characteristic response time of the $WASP_{12}$ index. This important caveat aside, for both drought and excessive wetness, Fig. 4 indicates that all three levels of severity appear to occur at roughly the same time, each following the peak strength of ENSO events. While it is well known that tropical land areas, on average, tend to be drier than average during El Niño, with the opposite occurring during La Niña (e.g., New et al. 2001), the relative sharpness of the peaks in the time series of Fig. 4 is nonetheless striking. Typical ENSO teleconnections sometimes fail to develop during individual events regardless of strength (e.g., Goddard et al. 1998) and ENSO is clearly only one factor among many affecting interannual climate conditions in the Tropics.

The strength of individual La Niña episodes was compared with the associated peak spatial extent of excessive wetness conditions for the nine events identified in the study period. These results are compared with the peak extent of drought during the ten strongest El Niño events in Fig. 5. The spatial extent of excessively wet conditions, for all levels of severity, is generally seen to also increase with the magnitude of below

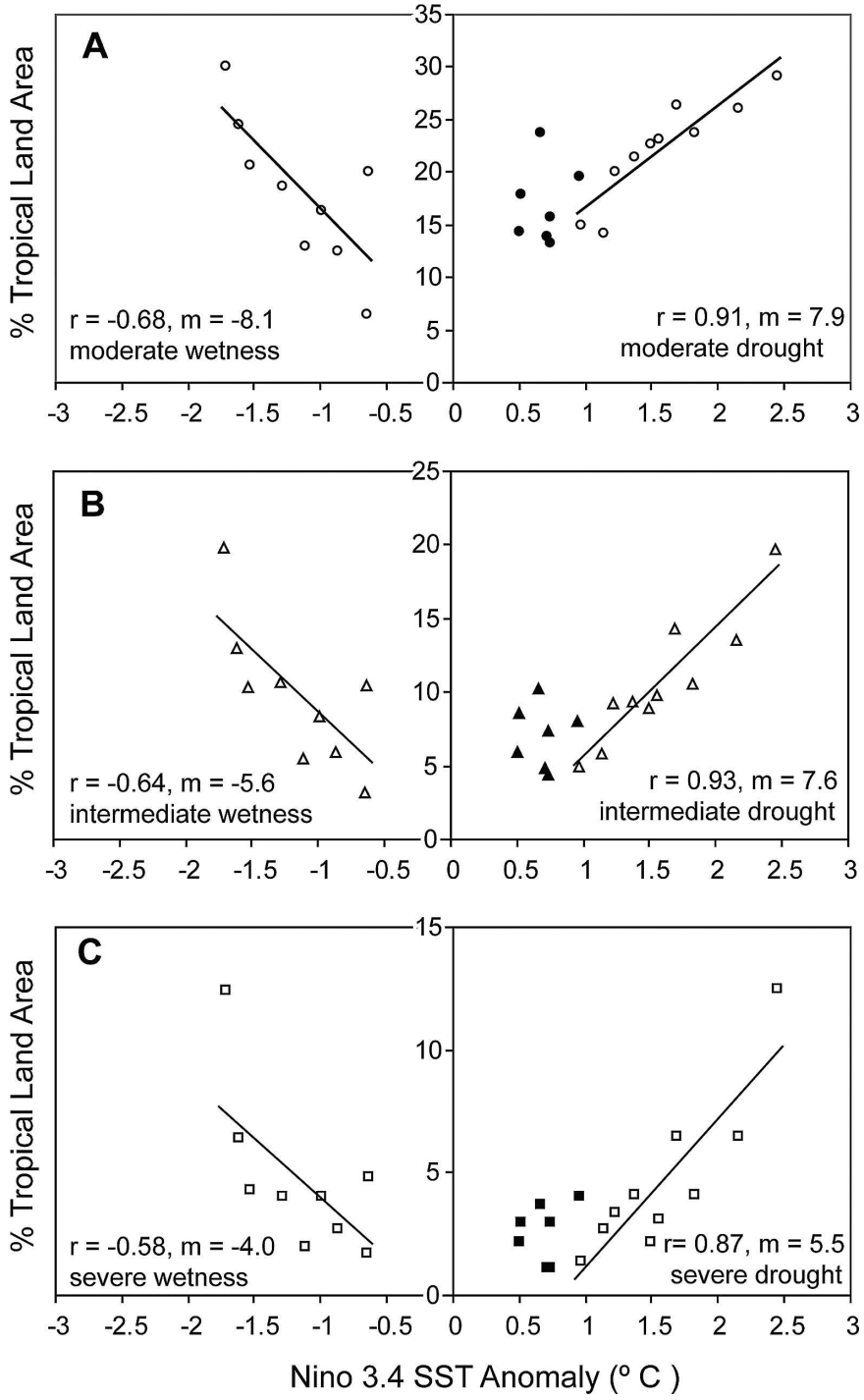

FIG. 5. Linear regression analyses for the maximum spatial extent (% of tropical land area) of (left) excessively wet conditions and (right) drought and the corresponding peak Niño-3.4 SST anomalies (°C) for associated ENSO events. Plots are for three levels of severity: (a) moderate (circles), (b) intermediate (triangles), and (c) severe (squares). The corresponding linear correlations and slopes are listed in the bottom of each of the plots. Solid symbols indicate data that were not used in computing the regressions and refer to seven weak El Niño events (listed in the appendix).

average Niño-3.4 SST anomalies. Although the correlations are not as high as for the case of drought during El Niño (~0.6 for La Niña; 0.8–0.9 for El Niño), the slopes of the regression lines are similar. Given the greater range of Niño-3.4 SST anomalies during El Niño events (1.50°C) compared with La Niña (1.11°C), the difference in correlations might be expected on mathematical grounds (restricting the range of a predictor reduces its correlation with the predictand) while on physical grounds the few, strong El Niño events might intuitively be expected to exert a greater forcing than their comparatively weaker, cold event counterparts. If the analysis for drought extent during El Niño is performed using a restricted range of Niño-3.4 SST anomalies in order to match those observed during La Niña events, correlations drop to the 0.6–0.7 range. However, it is noteworthy that two of the major peaks in the spatial extent of excessively wet conditions (ranking as the third and sixth largest in the 1950–98 time period) did not occur during La Niña events, with associated Niño-3.4 SST anomalies only slightly below average in those cases.

In Fig. 6 maps of composite values of the $WASP_{12}$ index are provided to give a Tropics-wide view (land and ocean) of the spatial patterns of drought and excessive rainfall associated with the warm and cold extreme phases of ENSO. The plots cover the 12-month period starting in April of the ENSO onset year and ending in March of the following year. The composite analyses are based on the CMAP data and include the six El Niño and four La Niña events occurring after 1979 (see the appendix). For comparison, similar analyses are shown for individual cases of strong El Niño (1997–98; Fig. 6b) and La Niña (1988–89; Fig. 6d) events. Many of the well-known teleconnection patterns are seen in the plots as well as a relative increase in the severity and spatial extent of rainfall extremes during the strong events.

b. *Timing of the peak spatial extent of moderate versus severe $WASP_{12}$ values*

As suggested in Fig. 4, there is typically a lag between the time of peak ENSO-related Niño-3.4 SST anomalies and the corresponding maximum spatial extent of drought or excessive wetness. However, it is not clear whether *severe* drought or wetness conditions should take longer to develop than *moderate* levels of these conditions. As shown in Fig. 7, no systematic tendency was found for the spatial extent of severe drought or wetness conditions to develop later than the intermediate or moderate categories of these respective conditions in the tropical average ENSO response. In addition, given the typical life cycle of ENSO events, attaining maximum strength (in terms of Niño-3.4 SST anomalies) during the late boreal fall into winter, the peak in spatial extent of precipitation extremes tends to occur from boreal fall onward. There is some suggestion that the peak spatial extent of excessively wet conditions (Fig. 7b) may tend to occur later in the year than drought conditions (based on a binomial distribution, the probability is ~ 0.03 of having so few occurrences of peak spatial extent of excessively wet conditions occurring between September and January), although in any given month local or regional precipitation extremes in the Tropics that are not related to ENSO influence the timing of the Tropics-wide spatial coverage.

c. *Enhanced likelihood of drought or excessive wetness during ENSO extremes*

Since, to lowest order, ENSO teleconnections tend to be collocated in space but of opposite sign (see Hoerling et al. 1997 and Hoerling et al. 2001 for important exceptions), in teleconnected land regions there would appear to be a bias toward one precipitation extreme or the other, depending upon the phase of ENSO. However, warm and cold ENSO events combined only occur about 50% of the time while drought and excessively wet conditions continue to develop in their absence, with the underlying mechanisms operating on a variety of temporal and spatial scales. For example, the protracted drought in the Sahel has been related to decadal-scale variability and trends in SST in the Atlantic and Indian Oceans (Giannini et al. 2003) and SSTs in the Indian Ocean have also been shown to influence seasonal climate in eastern and southern Africa independent of ENSO (Goddard and Graham 1999). Thus the full extent to which, locally, ENSO influences the relative likelihood of either drought or excessively wetness conditions is not clear and was therefore examined.

To indicate how this part of the analysis was performed, the case of assessing the likelihood of drought during El Niño (relative to all other times) is described. The same approach was taken for the alternative cases of El Niño and excessive wetness, La Niña and drought, and La Niña and excessive wetness. First, based on the Niño-3.4 SST time series, the total number of months that a given grid point was in drought during El Niño conditions was determined for all El Niño events during the period December 1950–December 1998. The "start" of an ENSO event was defined as the first month that the Niño-3.4 SST index exceeded the ±0.4°C threshold used to define such events. Given this definition, a 5-month lag following the start of an ENSO event was taken as the starting month in the $WASP_{12}$ time series (i.e., Niño-3.4 leading) to check for

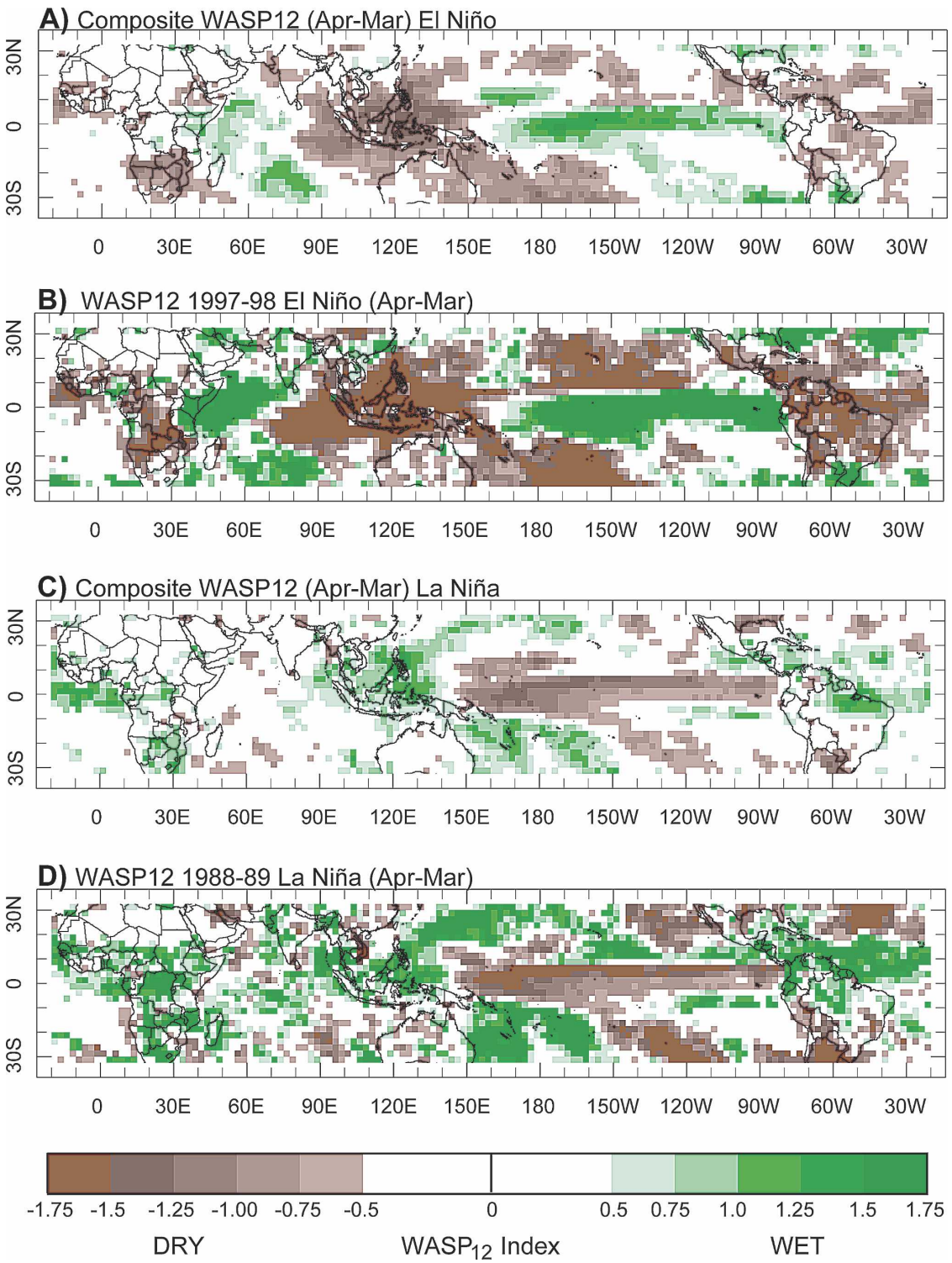

FIG. 6. Composite and case values of the $WASP_{12}$ index computed for the period from Apr of the onset year to Mar of the following year for (a) six El Niño events, (b) the 1997–98 El Niño, (c) four La Niña events, and (d) the 1988–89 La Niña.

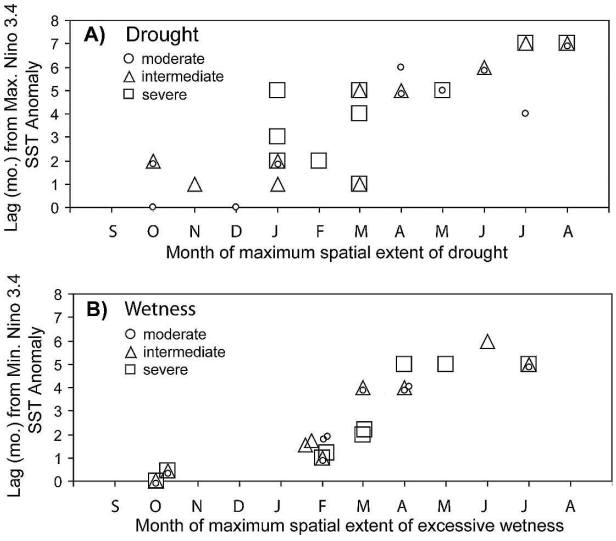

FIG. 7. Scatterplots of the lag (in months) between the peak value of Niño-3.4 SST anomalies and the corresponding calendar month when the peak in the spatial extent of (a) drought and (b) excessive wetness was observed for the 10 strongest El Niño, and 9 La Niña events, respectively. Three levels of severity are considered for each extreme as listed in the upper left of the plots.

drought/excessively wet conditions at each grid point. Again, while for some specific locations this may not be an optimal method for detecting the ENSO signal, it does capture large-scale patterns on a Tropics-wide basis. Only those grid points where the number of months in drought during El Niño exceeded those expected by chance (at 95% confidence, based on the assumption of the $WASP_{12}$ being approximately normally distributed) were retained. Then, to further emphasize the strength of the relationship, the ratio of the total number of months a given grid point was in drought (for a given threshold of severity) during El Niño conditions to the total number of months in drought (of the same severity) at all other times was computed. It turns out that ratio values >1 indicate, statistically, that drought is more likely during El Niño (relative to chance, $p < 0.05$). Moreover, in passing this statistical test, the total number of months in drought during El Niño (occurring 31% of the time) is greater than that observed in all other months (69% of the time).[3] This ratio is plotted in Fig. 8 for the severe categories of both drought and excessive wetness. The figure indicates that in several of the well-known teleconnected regions of the Tropics the likelihood of severe drought or wetness is significantly increased during ENSO, with the relative occurrence in some cases being greater by as much as a factor of 5. The areal extent of the Tropics for which drought (excessive wetness) is enhanced during El Niño (La Niña) was computed for all three categories of severity. It was found (not shown) that a much greater area of the Tropics is likely to experience severe drought (severe wetness) conditions during El Niño (La Niña) than moderate drought (moderate wetness) conditions. The areal coverage of the Tropics where drought or excessive wetness is more likely during ENSO events increases by roughly a factor of 2 for severe versus moderate categories of these extremes.

4. Summary and discussion

Given the design of the $WASP_{12}$ index, the *average* spatial coverage of respective positive and negative values will be essentially the same when the *entire* study period is considered (i.e., at a given grid point the WASP index is approximately Gaussian). However, since ENSO events occur only about half the time, this need not be the case for peak spatial coverage averaged over individual cold or warm ENSO events. This was nonetheless found to be approximately true for all three categories of respective wet and dry conditions (cf. Fig. 4). Major peaks in the spatial extent of drought since 1950 were closely associated with El Niño events having proportionately large Niño-3.4 SST anomalies, with a somewhat weaker association between La Niña and excessively wet conditions (e.g., two significant peaks in the spatial extent of wet conditions were not associated with La Niña, whereas all major peaks in drought extent were associated with El Niño). However, given the small number of ENSO events observed in the study period, no statistically significant differences in the relationship between the spatial extent of positive and negative precipitation extremes and the extreme phases of ENSO could be established. While the main focus of this study is on the spatially integrated effect of ENSO extremes on tropical land area precipitation, a related question to ask is whether the results found here are due to systematic, large-scale shifts in precipitation over the tropical oceans as well. Of course, observations of global-scale shifts in tropical precipitation (and other fields) are precisely what fueled early investigations of the ENSO phenomenon (e.g., Rasmusson and Carpenter 1982; Wallace et al. 1998) to begin with. However, the lack of rainfall data over tropical ocean areas has prevented an analysis of the spatial extent of precipitation anomalies over the oceans to be considered until only recently. In related work, satellite observations and derived products have been used by investigators to identify ENSO signatures in interannual variations of outgoing longwave radia-

[3] Given its design, there is a high autocorrelation between monthly values of the $WASP_{12}$ index. However, there is no a priori reason to expect that this autocorrelation should be greater during El Niño than for any other time.

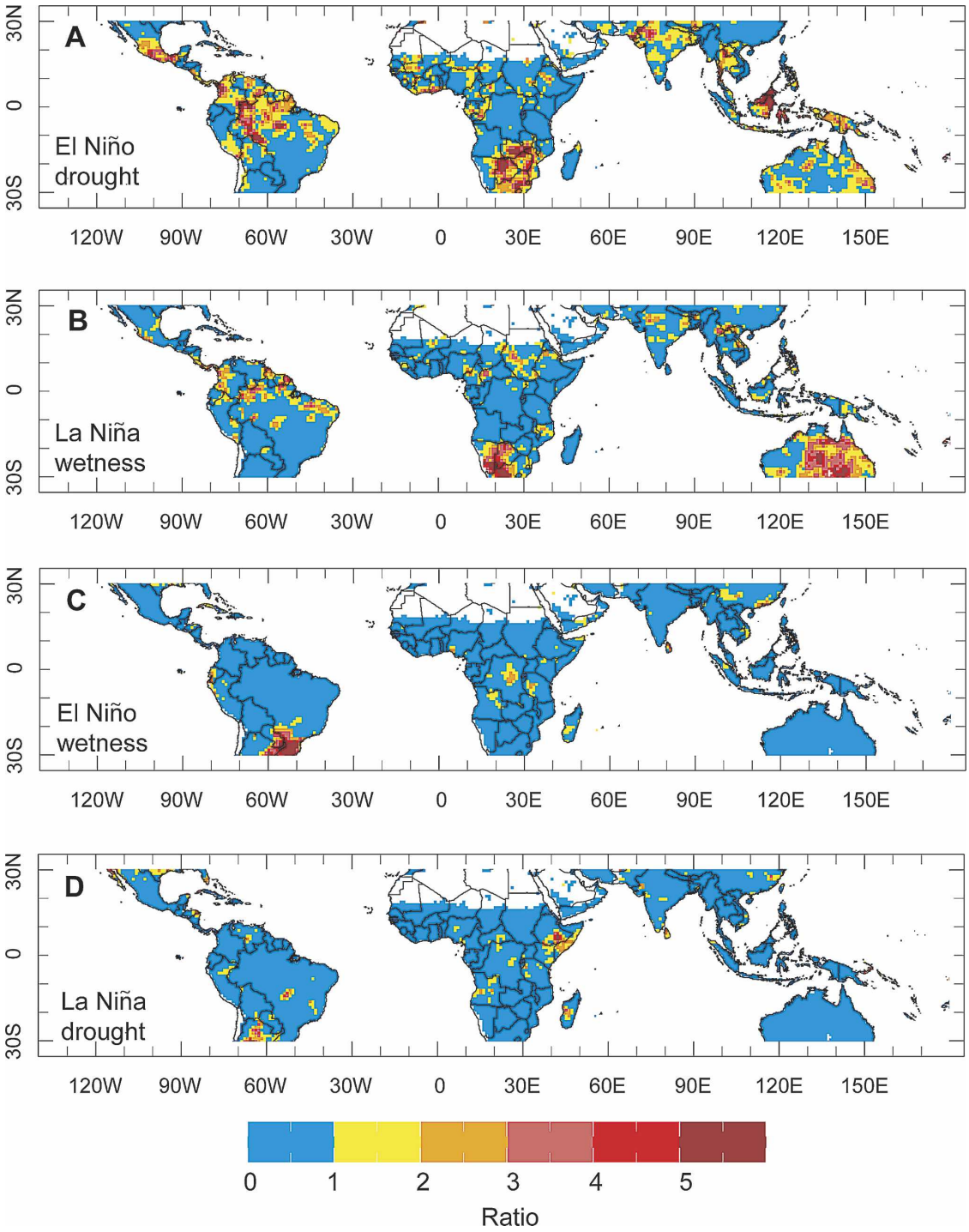

FIG. 8. Spatial distribution for the ratio of the total number of months a grid point was in the severe category of either wetness or drought during ENSO events to the total number of months this condition was true for all other times. Four different cases are plotted: (a) severe drought during El Niño, (b) severe wetness during La Niña, (c) severe wetness during El Niño, and (d) severe drought during La Niña. For grid points where the plotted ratio is >1 the probability of wet or dry extremes during ENSO events also had to be greater than that expected by chance (at the 0.05 level). See text for more details.

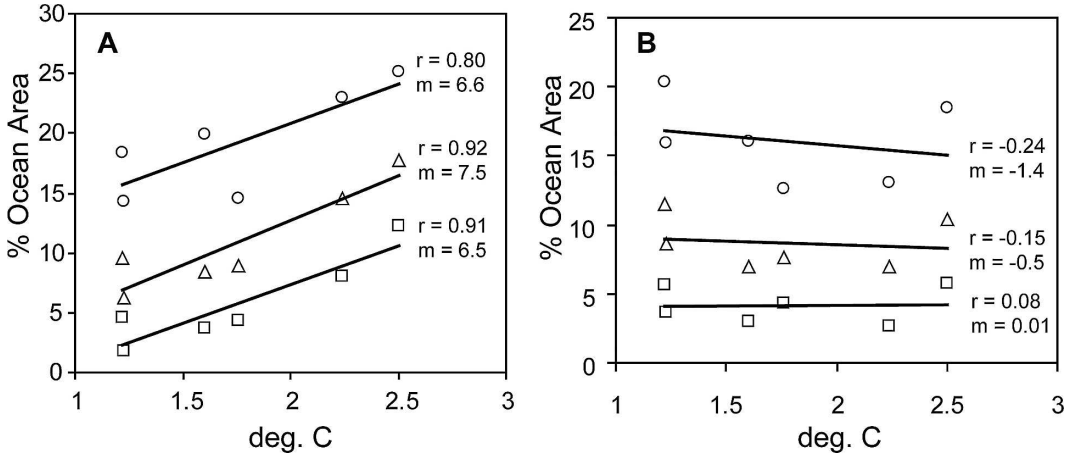

FIG. 9. Peak spatial extent (% area) of excessively wet conditions for tropical ocean areas during six El Niño events as a function of associated maximum Niño-3.4 SST anomalies (°C). In (a) all ocean areas are examined; in (b) the region (10°S–10°N, 150°E–80°W) has been excluded from the analysis. Three levels of severity are considered (symbols the same as those used in Fig. 5) and the linear correlation and slope of each regression line is indicated. Analysis based on the GPCP data for the period 1979–2003.

tion (OLR) across the Tropics (e.g., Chelliah and Arkin 1992; Yulaeva and Wallace 1994), and in monthly satellite estimates of precipitation for the globe (Dai and Wigley 2000; New et al. 2001). General circulation models (GCMs) have also been widely used to examine the influence of tropical SST anomalies on precipitation, although some noticeable disagreements with satellite rainfall estimates have been made in terms of the magnitude of response (e.g., Soden 2000). In none of these studies has the spatial extent of precipitation extremes been examined explicitly, or compared across multiple ENSO events. Here we utilize the GPCP data to perform an analysis similar to what was done for land regions, but for the period 1979–2003. Six El Niño and four La Niña events were identified during this period (see the appendix). While the sample size is clearly quite limited, this period witnessed ENSO events of varying strength including two strong El Niño (1982–83, 1997–98) and La Niña (1988–89, 1998–2000) events. If the manifestation of ENSO extremes on tropical land area precipitation results from a simple shift in large-scale precipitation patterns between ocean and land, one would expect to see an increase in the spatial extent of excessively wet (dry) conditions over the tropical oceans during El Niño (La Niña). Utilizing the $WASP_{12}$ index computed from satellite-derived GPCP monthly rainfall estimates, Fig. 9a displays the maximum spatial extent of excessively wet conditions during El Niño over the tropical oceans (only) as a function of associated maximum Niño-3.4 SST anomalies. The figure indicates a very good correspondence, with linear correlations of 0.8 or greater for all categories of severity of $WASP_{12}$ (for this sample size, $r > 0.8$ is statistically significant with >90% confidence). Of course, a trademark signature of El Niño events is the eastward shift of convection from the Maritime Continent eastward into the east–central tropical Pacific. Physically, increasingly positive SST anomalies in the Niño-3.4 region (and eastward) bring the total SSTs in an increasingly larger area of the Pacific cold tongue to the convective threshold (e.g., Hoerling et al. 2001), increasing the spatial extent of excessive wetness. However, a typical lagged response to El Niño includes a warming of SSTs averaged across the tropical oceans (e.g., Klein et al. 1999) and an increase in tropical ocean rainfall might be expected in other ocean regions as well. To check this, results obtained after excluding the east–central tropical Pacific (10°S–10°N, 150°E–80°W) from the analysis are displayed in Fig. 9b. The figure indicates there is no longer a consistent relationship between the spatial extent of excessively wet conditions over the tropical ocean and the magnitude of Niño-3.4 SST anomalies during El Niño. From the limited sample of events, the results suggest that the large-scale eastward shift of tropical convection in the tropical Pacific is the core ENSO precipitation response, with shifts in rainfall patterns elsewhere over the tropical oceans likely complicated by additional influences. Similar analyses performed for the spatial extent of dry conditions over the tropical oceans during four La Niña events are shown in Fig. 10. While the sample size is extremely limited, there is a suggestion of a good linear relationship between the spatial extent of dry conditions and the magnitude of Niño-3.4 SST anomalies, even when

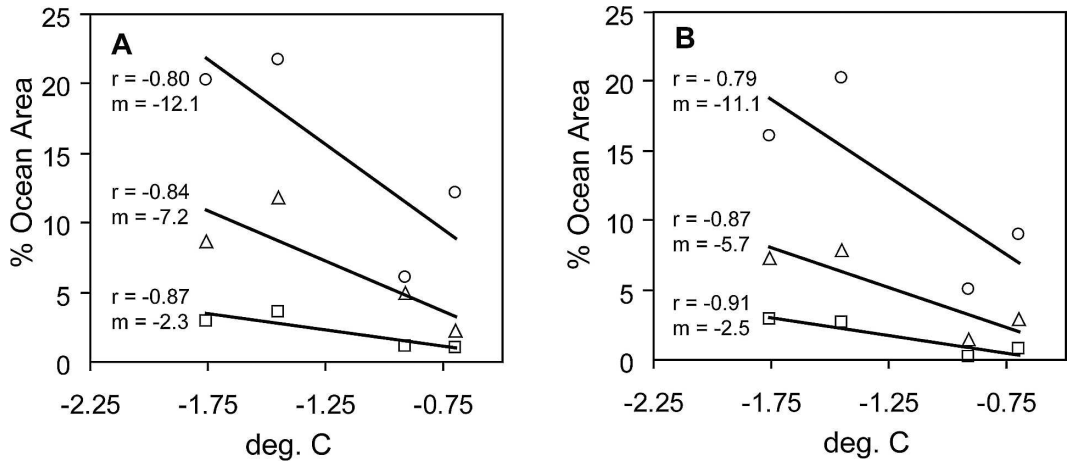

FIG. 10. As in Fig. 8 but for the four La Niña events identified during the period.

the east–central tropical Pacific is excluded from the analysis. The implied asymmetric behavior between warm and cold ENSO events after removing the east–central Pacific from the analysis is likely related to the fact that while increasingly large positive SST anomalies are able to bring total SSTs in the cold tongue region closer to their convective threshold, increasing negative SST anomalies only serve to reinforce the climatological, dry condition there.

Why maxima in the spatial extent of drought or excessively wet conditions should be expected to show a linear relationship to the magnitude of peak Niño-3.4

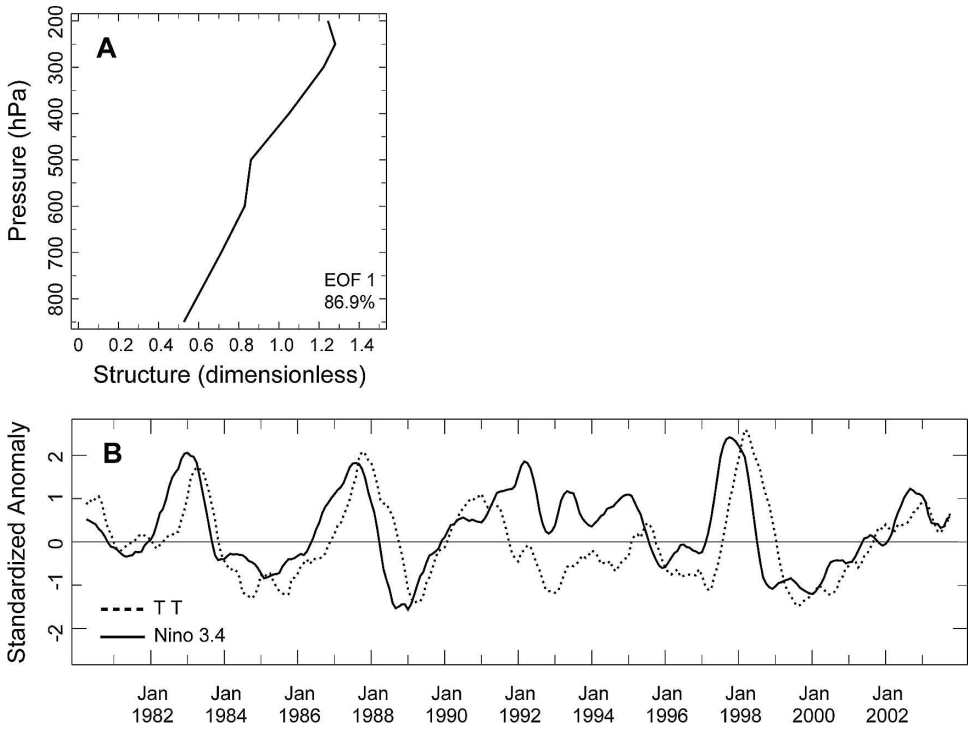

FIG. 11. (a) Vertical structure (dimensionless, magnitude arbitrary) and (b) standardized time series (dashed line) of the leading EOF of monthly tropical tropospheric temperature anomalies (850–200 hPa) averaged from 30°S to 30°N. The solid line in (b) is the standardized Niño-3.4 SST anomaly index for the corresponding period of Jan 1980–Dec 2003. Both time series in (b) have been smoothed using a 5-month running average.

SST is an important question in its own right. One idea, based on recent theoretical and modeling work by Chiang and Sobel (2002) and Neelin et al. (2003), is to conceptualize tropical ENSO forcing through variations in the tropical tropospheric temperature (TT). In this framework, the TT anomalies are at the core of ENSO precipitation teleconnections, which are then modified regionally by a host of contributing factors including the characteristics of the underlying surface, local wind and SST patterns, land–atmosphere interactions, etc. This TT anomaly forcing has a strong linear relationship with Niño-3.4 SST (Su et al. 2003) and more generally, with tropically averaged SST (Sobel et al. 2002). An EOF analysis was performed on the tropical tropospheric temperature field in the NCEP–NCAR reanalysis (850–200 hPa; averaged over all longitudes between 30°S and 30°N) to examine its association with the spatial extent of drought. The vertical structure and time series of the leading EOF of the TT anomaly field (explaining over 86% of the variance) is shown in Fig. 11 for the period 1980–2003. The figure indicates an imposed stabilizing profile of tropospheric temperature during El Niño similar to that reported by Chiang and Sobel (2002), with the opposite situation occurring during La Niña. The linear correlation between the EOF time series and Niño-3.4 SST anomalies is 0.8, consistent with expectations. For the limited number of El Niño events during the period, the linear correlation between maximum TT anomaly and peak spatial extent of drought is typically ~0.9 for all three levels of severity (not shown). Despite these high correlations, Niño-3.4 SST anomalies are highly correlated with TT anomalies, and the results of this simple comparison, while suggestive, cannot separate out what is merely a consistent relationship from an actual forcing mechanism. In addition, the behavior of TT anomalies is complicated by the volcanic eruptions of El Chichón in 1982 and Mount Pinatubo in 1991 (e.g., Fernández et al. 2004), and only a single maxima in TT anomalies was observed during the early 1990s. Nonetheless, the high correlations between TT anomalies and drought extent over land are an interesting finding. Finally, based on the magnitude of their associated Niño-3.4 SST anomalies, four of the five largest El Niño events in the study period have occurred since 1980. These events were associated with the greatest spatial extent of drought in tropical land areas during that period. While increasing global surface air temperatures have recently been linked to increasing drought extent over global land areas (Dai et al. 2004), the results of the current study suggest that the future behavior of El Niño will likely be a significant factor in determining the spatial extent of drought in the Tropics in the future, at least on interannual time scales, with increasing surface air temperatures likely acting to exacerbate those conditions.

Acknowledgments. The authors thank A. Sobel, L. Goddard, and S. Mason for their comments, suggestions, and insights on various aspects of this study. The comments of two anonymous reviewers and the editor served to clarify a number of points and to greatly improve the original version of this manuscript. The IRI is supported by NOAA and the Columbia University and is part of the Columbia Earth Institute.

APPENDIX

General Characteristics of Historical ENSO Events

The El Niño (La Niña) events used in the study are listed below. The dates for the onset–demise of each event are based on the month where the maximum (minimum) Niño-3.4 SST anomaly index crosses the ±0.4°C threshold used to define events (see section 2c).

Onset–demise of the 10 strongest El Niño events			
	Duration (month)	Maximum Niño-3.4 SST anomaly (°C)	Date of maximum SST anomaly
Apr 1997–May 1998	14	2.50	Nov 1997
Apr 1982–Jun 1983	15	2.24	Dec 1982
May 1972–Mar 1973	11	1.92	Nov 1972
Nov 1990–Jul 1992	21	1.76	Feb 1992
Aug 1986–Feb 1988	19	1.60	Sep 1987
Jun 1965–May 1966	12	1.53	Oct 1965
Apr 1957–Jun 1958	15	1.48	Jan 1958
Mar 2002–Mar 2003	13	1.23	Nov 2002
Mar 1994–Apr 1995	14	1.22	Dec 1994
Sep 1968–Feb 1970	18	1.00	Feb 1969
Additional El Niño events			
Jun 1963–Feb 1964	9	0.96	Nov 1963
Jul 1977–Feb 1978	8	0.80	Nov 1977
Feb 1993–Aug 1993	7	0.79	May 1993
Sep 1976–Mar 1977	7	0.76	Dec 1976
Aug 1951–Jan 1952	6	0.67	Oct 1951
Mar 1953–Sep 1953	7	0.54	Jun 1953
Oct 1979–Mar 1980	6	0.53	Nov 1979
Onset–demise of 9 La Niña events			
Jun 1973–Apr 1976	35	−1.79	Dec 1973
May 1988–May 1989	13	−1.76	Dec 1988
May 1954–Dec 1956	32	−1.65	Oct 1955
Jul 1998–Jun 2000	24	−1.45	Dec 1999
Jul 1970–Jan 1972	19	−1.18	Feb 1971
May 1964–Feb 1965	10	−1.04	Oct 1964
Sep 1984–Jul 1985	11	−0.91	Jan 1985
Sep 1995–Feb 1996	6	−0.70	Dec 1995
Nov 1967–Apr 1968	6	−0.68	Mar 1968

REFERENCES

Alley, W. M., 1984: The Palmer drought severity index: Limitations and assumptions. *J. Climate Appl. Meteor.,* **23,** 1100–1109.

Barnston, A. G., M. Chelliah, and S. B. Goldenberg, 1997: Documentation of a highly ENSO-related SST region in the equatorial Pacific. *Atmos.–Ocean,* **35,** 367–383.

Chelliah, M., and P. Arkin, 1992: Large-scale interannual variability of monthly outgoing longwave radiation anomalies over the global tropics. *J. Climate,* **5,** 371–389.

Chen, M., P. Xie, J. E. Janowiak, and P. A. Arkin, 2002: Global land precipitation: A 50-yr monthly analysis based on gauge observations. *J. Hydrometeor.,* **3,** 249–266.

Chiang, J. C. H., and A. H. Sobel, 2002: Tropical tropospheric temperature variations caused by ENSO and their influence on the remote tropical climate. *J. Climate,* **15,** 2616–2631.

Dai, A., and T. M. L. Wigley, 2000: Global patterns of ENSO-induced precipitation. *Geophys. Res. Lett.,* **27,** 1283–1286.

——, I. Y. Fung, and A. D. Del Genio, 1997: Surface observed global land precipitation variations during 1900–88. *J. Climate,* **10,** 2943–2962.

——, K. E. Trenberth, and T. R. Karl, 1998: Global variations in droughts and wet spells: 1900–1995. *Geophys. Res. Lett.,* **25,** 3367–3370.

——, ——, and T. Qian, 2004: A global dataset of Palmer drought severity index for 1870–2002: Relationship with soil moisture and effects of surface warming. *J. Hydrometeor.,* **5,** 1117–1130.

Dilley, M., and B. N. Heyman, 1995: ENSO and disaster: Droughts, floods and El Niño/Southern Oscillation warm events. *Disasters,* **19,** 181–193.

Fernández, N. C., R. R. García, R. G. Herrera, D. G. Puyol, L. G. Presa, E. H. Martín, and P. R. Rodriguez, 2004: Analysis of the ENSO signal in tropospheric and stratospheric temperatures observed by MSU, 1979–2000. *J. Climate,* **17,** 3934–3946.

Giannini, A., R. Saravanan, and P. Chang, 2003: Ocean forcing of Sahel rainfall on interannual to interdecadal time scales. *Science,* **302,** 1027–1030.

Goddard, L., and N. E. Graham, 1999: Importance of the Indian Ocean for simulating rainfall anomalies over eastern and southern Africa. *J. Geophys. Res.,* **104,** 19 099–19 116.

——, S. Mason, N. Graham, and W. Thaiw, 1998: Climate surprises of the 1997/98 El Niño. *Proc. 23d Annual Climate Diagnostics and Prediction Workshop,* Miami, FL, NOAA/Climate Prediction Center–RSMAS, University of Miami, 34–37.

Hartman, D. L., 1994: *Global Physical Climatology*. Academic Press, 411 pp.

Hoerling, M. P., A. Kumar, and M. Zhong, 1997: El Niño, La Niña, and the nonlinearity of their teleconnections. *J. Climate,* **10,** 1769–1786.

——, ——, and T. Xu, 2001: Robustness of the nonlinear climate response to ENSO's extreme phases. *J. Climate,* **14,** 1277–1293.

Hu, Q., and G. D. Wilson, 2000: Temperature effects on the Palmer Drought Severity Index. *Int. J. Climatol.,* **20,** 1899–1911.

Huffman, G. J., and Coauthors, 1997: The Global Precipitation Climatology Project (GPCP) combined precipitation dataset. *Bull. Amer. Meteor. Soc.,* **78,** 5–20.

Kiladis, G. N., and H. F. Diaz, 1989: Global climate anomalies associated with extremes in the Southern Oscillation. *J. Climate,* **2,** 1069–1090.

Kistler, R., and Coauthors, 2001: The NCEP–NCAR 50-Year Reanalysis: Monthly means CD-ROM and documentation. *Bull. Amer. Meteor. Soc.,* **82,** 247–268.

Klein, S., B. J. Soden, and N.-C. Lau, 1999: Remote sea surface temperature variations during ENSO: Evidence for a tropical atmospheric bridge. *J. Climate,* **12,** 917–932.

Lyon, B., 2004: The strength of El Niño and the spatial extent of tropical drought. *Geophys. Res. Lett.,* **31,** L21204, doi:10.1029/2004GL020901.

Mason, S. J., and L. Goddard, 2001: Probabilistic precipitation anomalies associated with ENSO. *Bull. Amer. Meteor. Soc.,* **82,** 619–638.

Neelin, J. D., C. Chou, and H. Su, 2003: Tropical drought regions in global warming and El Niño teleconnections. *Geophys. Res. Lett.,* **30,** 2275–2278.

New, M., M. Hulme, and P. D. Jones, 1999: Representing twentieth century space–time climate variability. Part I: Development of a 1961–90 mean monthly terrestrial climatology. *J. Climate,* **12,** 829–856.

——, ——, and ——, 2000: Representing twentieth century space–time climate variability. Part II: Development of 1901–96 monthly grids of terrestrial surface climate. *J. Climate,* **13,** 2217–2238.

——, M. Todd, M. Hulme, and P. D. Jones, 2001: Precipitation measurements and trends in the twentieth century. *Int. J. Climatol.,* **21,** 1899–1922.

Rasmusson, E. M., and T. H. Carpenter, 1982: Variations in tropical sea surface temperature and surface wind fields associated with the Southern Oscillation/El Niño. *Mon. Wea. Rev.,* **110,** 354–384.

Ropelewski, C. F., and M. H. Halpert, 1987: Global and regional scale precipitation patterns associated with the El Niño–Southern Oscillation. *Mon. Wea. Rev.,* **115,** 1606–1626.

Smith, T. M., and R. W. Reynolds, 2003: Extended reconstruction of global sea surface temperatures based on COADS data (1854–1997). *J. Climate,* **16,** 1495–1510.

Sobel, A. H., I. M. Held, and C. S. Bretherton, 2002: The ENSO signal in tropical tropospheric temperature. *J. Climate,* **15,** 2702–2706.

Soden, B. J., 2000: The sensitivity of the tropical hydrological cycle to ENSO. *J. Climate,* **13,** 538–549.

Su, H., J. D. Neelin, and J. E. Meyerson, 2003: Sensitivity of tropical tropospheric temperature to sea surface temperature forcing. *J. Climate,* **16,** 1283–1301.

Trenberth, K. E., 1997: The definition of El Niño. *Bull. Amer. Meteor. Soc.,* **78,** 2771–2777.

Wallace, J. M., E. M. Rasmusson, T. P. Mitchell, V. E. Kousky, E. S. Sarachik, and H. von Storch, 1998: On the structure and evolution of ENSO-related climate variability in the tropical Pacific: Lessons from TOGA. *J. Geophys. Res.,* **103,** 14 241–14 259.

Xie, P., and P. A. Arkin, 1996: Analysis of global monthly precipitation using gauge observations, satellite estimates, and numerical model predictions. *J. Climate,* **9,** 840–858.

Yin, X., A. Gruber, and P. Arkin, 2004: Comparison of the GPCP and CMAP merged gauge–satellite monthly precipitation products for the period 1979–2001. *J. Hydrometeor.,* **5,** 1207–1222.

Yulaeva, E., and J. M. Wallace, 1994: The signature of ENSO in global temperature and precipitation fields derived from the Microwave Sounding Unit. *J. Climate,* **7,** 1719–1736.